Relaxation dynamics following transition of solvated electrons

R. B. Barnett and Uzi Landman
School of Physics, Georgia Institute of Technology, Atlanta, Georgia 30332

Abraham Nitzan
School of Chemistry, Sackler Faculty of Exact Sciences, Tel Aviv University, Tel Aviv 69978, Israel

(Received 16 December 1988; accepted 10 January 1989)

Relaxation dynamics following an electronic transition of an excess solvated electron in clusters and in bulk water is studied using an adiabatic simulation method. In this method the solvent evolves classically and the electron is constrained to a specified state. The coupling between the solvent and the excess electron is evaluated via the quantum expectation value of the electron–water molecule interaction potential. The relaxation following excitation (or deexcitation) is characterized by two time scales: (i) a very fast ($\sim$20–30 fs) one associated with molecular rotations in the first solvation shell about the electron, and (ii) a slower stage ($\sim$200 fs), which is of the order of the longitudinal dielectric relaxation time. The fast relaxation stage exhibits an isotope effect. The spectroscopical consequences of the relaxation dynamics are discussed.

I. INTRODUCTION

The dynamics of polar solvent reorganization associated with changes in the charge distribution of a solute species has been an active area of research in the last two decades.[1–3] Such studies deal with the dynamics of solvent relaxation associated with molecular excitation,[4–13] ionic solvation,[14–16] electron transfer[17–25] and electron localization[26–31] in polar solvents. Theoretical studies of these phenomena have usually involved a continuum dielectric model for the solvent, specified by its dielectric dispersion $\epsilon(\omega)$.[14,32–42] More recently several studies where the molecular nature of the solvent was accounted for in an approximate manner, have been published.[43–49] In particular, a combination of linear response theory with the dynamical mean spherical approximation (MSA), originally developed by Wolynes[47] and later further developed and applied by Rips, Klafter, and Jortner[48] and by Nichols and Calef,[49] was recently shown by Maroncelli and Fleming[50] to account well for the main trends in the experimental molecular fluorescence results.

An alternative approach to the dynamics of solvation phenomena is provided by numerical simulations and several such studies have been published for aqueous solutions.[15,16,51–53] Such studies, in particular the very detailed one by Maroncelli and Fleming[16] have provided much insight into the molecular nature of the solvation process. Their relevance to the actual experimental systems depends of course on the quality of the potential used. It should be pointed out that such simulations of aqueous solutions are of particular importance because the validity of simple models such as the MSA[14] is questionable for such a highly associated and highly structured solvent.

Technological advances in the creation and detection of ultrashort optical signals have made it now possible to follow solvation dynamics in such systems where the logitudinal dielectric relaxation time τ_L is $\lesssim$0.5 ps. In particular Migus *et al.*[29] have followed the subpicosecond evolution of the electron absorption spectrum following electron injection (by photoionization) in bulk water (following the $\sim$100 fs ionization pulse) where absorption in the near IR which seems to build up with a characteristic time of $\sim$110 fs, and a subsequent decay of this signal and a buildup of absorption in the $\lambda = 700$–900 nm region on a time scale of $\sim$240 fs were observed. The absorption spectrum seems not to exhibit a continuous shift from the infrared to the visible, and the authors propose that the absorptions in these two spectral regimes correspond to two distinct electronic species: One (the IR absorber) which forms on a time scale comparable to the duration of the ionizing pulse, and the other which is close to the fully hydrated electron.

Most recently Rossky and co-workers[53,54] have performed simulations of this system employing the SPC (simple point charge) water potential model and a pseudopotential for the electron–water interaction. The starting points of these simulations are ground states of the electron calculated for static water configurations selected from an equilibrium ensemble obtained in the absence of the electron. Analysis of the energy distribution associated with the ground and excited electronic states obtained for these neutral water configurations yields an absorption line shape which is consistent with the experimentally observed initial IR absorption. The subsequent time evolution is performed assuming adiabatic behavior, i.e., the electron is confined to stay in the ground state corresponding to the instantaneous nuclear configuration. This "ground-state dynamics" (GSD) evolution exhibits the following characteristics.

(a) The excess electron localizes to nearly its equilibrium radius within $\sim$30 fs. Coincidentally the energy drops by $\sim$2.5 eV. Further relaxation occurs on a larger time scale ($\sim$200 ps) after most of the binding energy has already been reached.

(b) The calculated spectra show a continuous blue shift from the absorption in the IR at $t = 0$ to an absorption peaked about 700 nm which is characteristic to a fully hydrated electron. The spectral shape and its peak position become similar to that of the equilibrium absorption after $\sim$40 fs.

Based on the discrepancy between these results and experimental observation of Migus *et al.*,[29] Rossky and

 0021-9606/89/084413-10$02.10

Schnitker have concluded that the ground-state dynamics simulation is not adequate for the early stages of electron solvation in water and that the first species observed after the ionizing pulse in the Migus *et al.* experiment is a solvated excited state. They propose that the rate determining step in the subsequent evolution towards the fully hydrated electron in its ground state is the nonadiabatic transition from the excited to the ground state.

In order to gain further insight into the relaxation processes associated with the solvated electron and of the solvation process, we have performed adiabatic simulations of negatively charged water clusters following transitions of the excess electron between the ground electronic state and the lowest excited electronic state. We have simulated the cluster relaxation following a transition from the ground to the excited electronic state, as well as simulations following the reverse electronic transition, i.e., a deexcitation from the excited to the ground state. Most relevant to the results discussed above is the second relaxation process, however, we find that both of them behave quite similarly. In both cases the relaxation is seen to proceed in a nonexponential fashion with at least two time scales involved: a fast one ($\sim$20–30 fs for room-temperature clusters) during which the energy gap between the two electronic states changes to about 60% of its final value and the width of the electron wave function (the electron "radius of gyration") relaxes to approximately its final value, and a relatively slow ($\sim$250 fs) time scale during which the electronic energy gap becomes fully developed. These time scales are not strongly sensitive to the cluster size for $(H_2O)_n^-$ clusters which support internally bound ground and excited electronic states ($n \gtrsim 60$; actual simulations were done with $n = 64$ and $n = 128$). They are, however, strongly sensitive to deuterium isotope substitution and also depend on the cluster temperature.

Details of our simulation method are given in Sec. II and in the Appendix. The results of our simulations are presented and discussed in Sec. III.

II. THE SIMULATION PROCEDURE

The simulation procedure has been described in detail in previous publications,[55–57] thus we give here only a short summary. The water–water potential employed is the RWK2-M potential[58] which has been applied successfully in calculations of equilibrium properties and vibrational spectra of water and water clusters. The electron–water interaction[59] is modeled by a pseudopotential which includes coulomb, polarization, exclusion, and exchange contributions. This electron–water molecule pseudopotential has been used by us recently in studies of the cluster size dependence of the energetics, mode of localization and solvation,[60] migration,[57] and spectra[56] of electrons in water clusters, yielding results in agreement with available experimental data. The water molecules are treated classically. The classical equation of motions are integrated using the velocity version of the Verlet algorithm, and the quantum-mechanical evolution of the electronic wave function is performed using the fast Fourier transform (FFT) split-operator algorithm.[61] In the present work the electron is restricted to stay in one electronic state (which evolves adiabatically with the nuclear configuration). This adiabatic evolution is achieved by propagating the wave function in imaginary time followed by normalization until convergence is achieved. Such procedure yields the ground electronic state, or, when accompanied by a projection operator which removes lower electronic states after each imaginary timestep, the next lowest excited state. For a brief formal description of the adiabatic simulation method (ASM) see the Appendix.[55,56] (A different adiabatic evolution method was recently described by Sprik and Klein.[62]) The electron–water interaction enters into the electronic Hamiltonian as a potential which depends on the instantaneous positions of the nuclei, and into the classical equations of motion for the water molecules as an expectation value over the instantaneous electronic wave function. This wave function is the ground-state function when ground-state dynamics is executed, and the lowest excited state function when adiabatic evolution on the excited potential surface is explored. It should be pointed out that restricting the excited state evolution to the lowest electronic state is somewhat artificial: the energies of the three lowest p-like excited states are not far apart (thus while the average energy spacings between these states in the $(H_2O)_{128}^-$ are from our simulations $\sim$0.3 eV, these energies fluctuate with the cluster configurations and can become close to each other: We have observed typically 1–2 near crossing events, $\Delta E \lesssim kT$ for $T = 300$ K, between the first and second excited state in 1 ps trajectories) so that nonadiabatic transitions between them cannot be ruled out. However, such occurrences are rare on the simulation time scales discussed below and should not have an appreciable effect on the observed solvation dynamics.

The main technical details of the simulations are as follows: A timestep of 10 a.u. ($= 2.4\times10^{-16}$ s) is used for the classical particles using the velocity version of the Verlet algorithm. The grid used for the electronic wave functions of the $(H_2O)_{64}^-$ cluster consists of 32^3 points with grid spacing $a = 1.2$ a.u. and for the $(H_2O)_{128}^-$ cluster a 16^3 grid is used with $a = 1.5$ a.u. The need for a larger grid for the $(H_2O)_{64}^-$ cluster arises because the excited state wave function is relatively extended and is not described well on the smaller grid for this cluster size. The imaginary timestep for the electronic state relaxation was taken to be 0.6 a.u. Finally, our simulations are performed at constant temperature (canonical ensemble) via employment of the stochastic collision method where at each integration timestep of the classical subsystem the velocities of randomly selected atoms are thermalized according to a Maxwell–Boltzmann velocity distribution corresponding to the desired temperature. We have also run a few constant energy trajectories obtaining similar result.

Using this procedure we have generated nuclear trajectories for motion either on the ground or on the excited potential surface. The wave functions and the electronic energies associated with both electronic states are calculated along these trajectories, yielding the adiabatic evolutions of these quantities as well as related quantities such as the electronic vertical energy gap, the transition dipole moment between the two electronic states and the electron gyration

radius. Results of these caculations are presented and discussed in the next section.

III. RESULTS AND DISCUSSION

The calculations described below are aimed at elucidating the details of the time evolution of the nuclear configurations following a sudden switching from the ground to an excited electronic state or from the excited to the ground electronic state. To this end we have selected several equilibrium configurations of the $(H_2O)_{\bar{64}}$ and the $(H_2O)_{\bar{128}}$ clusters in the ground electronic state and followed the time evolution of the nuclear configuration and the associated electronic energies after switching, at time $t = 0$, from the ground to the excited electronic state. Thus starting from a ground-state configuration, the water molecules begin their motion on the (lowest) excited electronic potential surface and the subsequent evolutions of both the classical (water) and quantum (electronic) subsystems are followed. Subsequently, after full relaxation of the system on the excited state potential surface has been achieved, the electronic state is switched back to the ground state, and the subsequent relaxation to the ground-state configuration is observed.

Figure 1 depicts the time evolution of the ground (E_0) and the first excited (E_1) electronic energies of $(H_2O)_{\bar{64}}$ [Fig. 1(a)] and $(H_2O)_{\bar{128}}$ [Fig. 1(b)] clusters, following a sudden switch from the ground to the first excited state. Figure 2 shows the corresponding evolutions of the energy gaps ($\Delta E = E_1 - E_0$) in these clusters. The time-dependent widths [gyration radia $(\langle r^2\rangle - \langle r\rangle^2)^{1/2}$, where the expectation value is taken over the excess electron wave functions] of the ground and excited electronic state configurations for $(H_2O)_{\bar{128}}$ are depicted in Fig. 3. The time evolution of the transition dipols $|\mu_{ge}|^2$ between the ground and excited electronic states for the larger cluster is shown in Fig. 4.

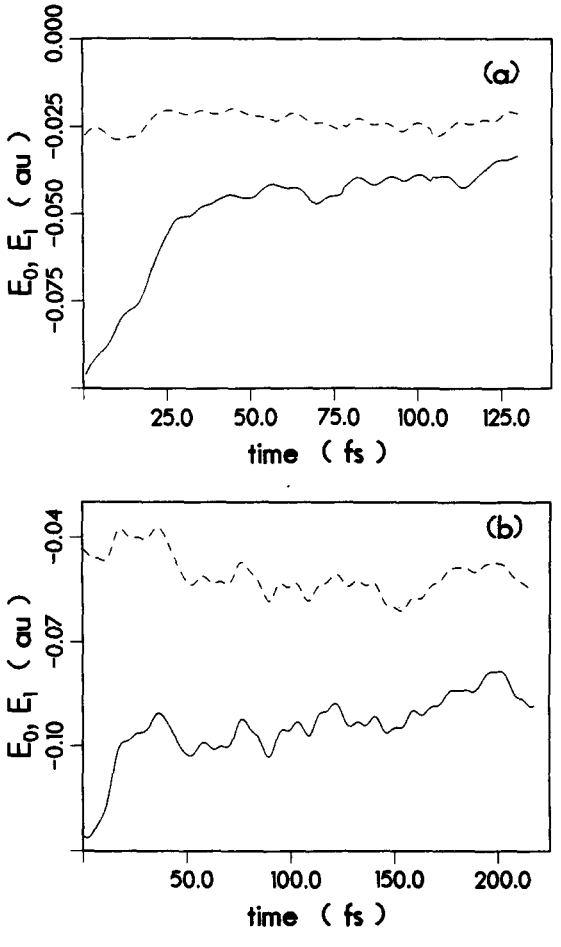

FIG. 1. Time evolution of the ground (E_0, solid line) and the first excited (E_1, dashed line) state energies of the solvated electron in $(H_2O)_{\bar{64}}$ (a) and in $(H_2O)_{\bar{128}}$ (b) following a sudden excitation (at $t = 0$) from the ground to the first excited state. The results, as well as those shown in Figs. 2–5, are averaged over five runs in each case.

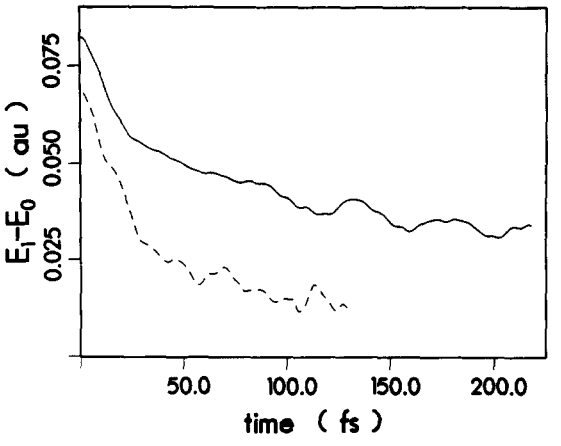

FIG. 2. Time evolution of the energy gap $\Delta E = E_1 - E_0$ for $(H_2O)_{\bar{64}}$ (dashed line) and $(H_2O)_{\bar{128}}$ (solid line) following a sudden excitation from (at $t = 0$) the ground to the first excited state.

All these quantities exhibit a typical time evolution characterized by a very fast initial relaxation on a timescale of ~20–30 fs, folowed by a slower relaxation process on a timescale of ~200–250 fs. A similar behavior is observed after a sudden switching back to the ground electronic state, shown for the state energies, the energy gap ΔE and the ground and excited state widths in Figs. 5(a)–5(c), respectively.

The slow (200–500 fs) component of the relaxtion pro-

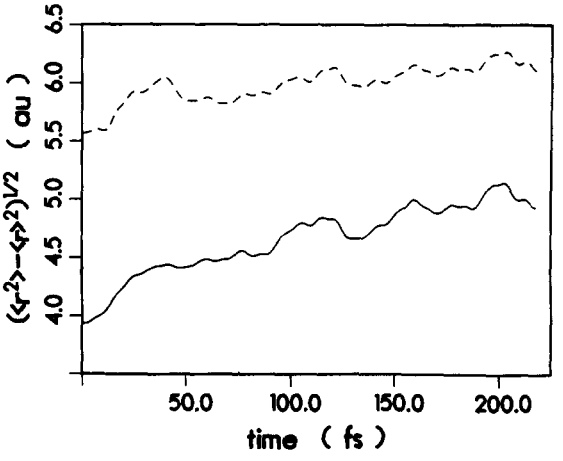

FIG. 3. The time evolution of the electron gyration radius $\sqrt{\langle r^2\rangle - \langle r\rangle^2}$, following (at $t = 0$) transition from the ground to the first excited state for $(H_2O)_{\bar{128}}$. Solid line: radius of the ground electronic state. Dashed line: radius of the excited state.

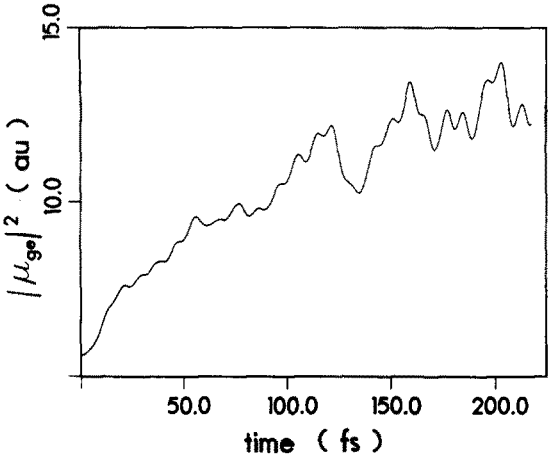

FIG. 4. Time evolution of the squared transition dipole, $|\mu_{ge}|^2$, between the ground and first excited state following transition to the excited state in $(H_2O)_{128}^-$. The transition dipole corresponding to the excited state configuration is larger because of the larger overlap between the corresponding wave functions.

cess seems to correspond to the longitudinal relaxation time (τ_L) of water, which is estimated to be in this range. The fast relaxation component is not predicted by contiuum dielectric theories[32–42] or by approximate methods (such as the mean spherical approximation, MSA)[44–49] which have been used to account for the microscopic solvent structure. In this context we note that that the behavior of the relaxation process seen in Figs. 1–5 bears close resemblance to the simulation results of Schnitker and Rossky[53] of an electron localization process described in Sec. I. This similarity is emphasized in Fig. 6 where results of a simulation similar to that of Ref. 53 but using our models for the water–water interaction (RWK2-M) and for the eletron–water pseudopotential, are shown. Figure 6(a) (solid curve) shows the time evolution of the ground-state energy of an electron starting in a preexisting trap in neutral bulk water (256 water molecules with periodic boundary conditions). In Fig. 6(b) (solid curve) we show the time evolution of the width of the electronic wave function for this process. As evident from Fig. 6(b), $\sqrt{\langle r^2\rangle - \langle r\rangle^2}$ reaches essentially its equilibrium value of ~ 4 a.u. after ~ 30 fs. We note that a similar fast process was observed by us in a simulation of electron localization at the surface of a large (256) water cluster.[57] It is interesting to note also that similar behavior is observed in classical computer simulations of water relaxation about a suddenly formed charge.[15,16,51,63]

To elucidate the nature of this fast relaxation process we also show in Fig. 6 the relaxation behavior of D_2O during the electron localization process (dashed curves). The two curves corresponding to H_2O and D_2O in Fig. 6 start both from the same initial configuration. While statistics are obviously poor, it appears that the fast relaxation time in D_2O is longer by $\sqrt{2}$. This conclusion is emphasized by the dotted lines in Figs. 6(a) and 6(b), where the results for D_2O are plotted versus time scaled by $2^{-1/2}$, i.e., the hydrogen to

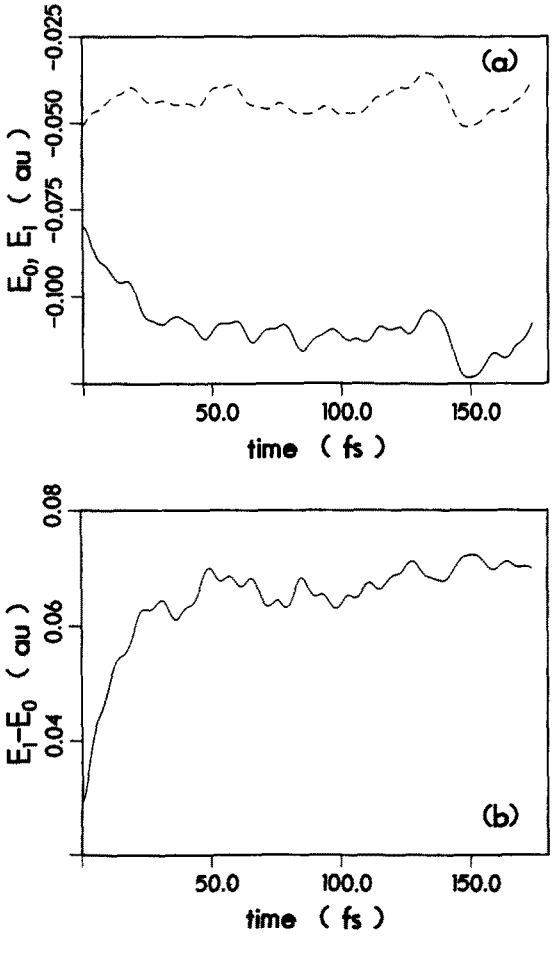

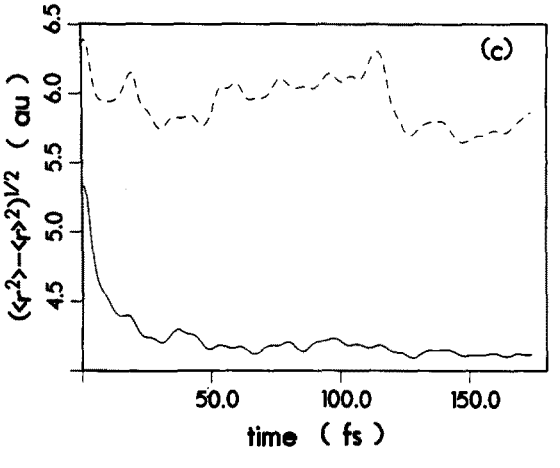

FIG. 5. Time evolution following a sudden transition (at $t = 0$) from the (equilibrated) first excited state to the ground electronic state. (a) Ground and excited state energies. (b) Energy gap. (c) Ground (solid line) and excited (dashed line) widths.

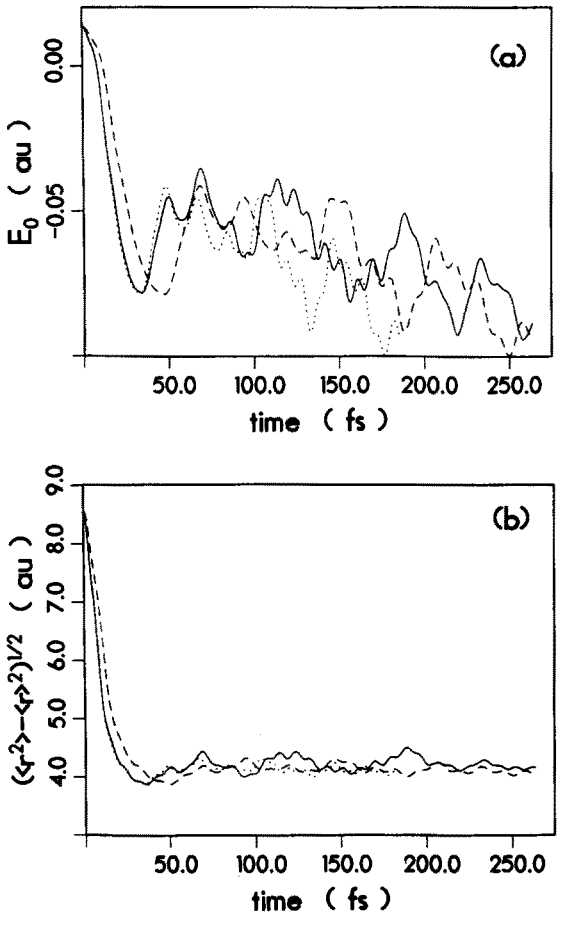

FIG. 6. (a) Time evolution of the ground-state energy of an excess electron during an adiabatic localization process in *bulk* liquid water. At $t = 0$ the electron starts from a preexisting trap in a neutral water configuration. (b) Time evolution of the width of the electronic wave functions $(\langle r^2\rangle - \langle r\rangle^2)^{1/2}$, during the same localization process. Solid lines: H_2O (256 molecules with periodic boundary conditions). Dashed lines: D_2O. Both the H_2O and the D_2O trajectories start from the same initial configuration. The dotted lines in (a) and (b) correspond to the D_2O curve with the time axis divided by $\sqrt{2}$ (i.e., the deuterium to hydrogen mass ratio).

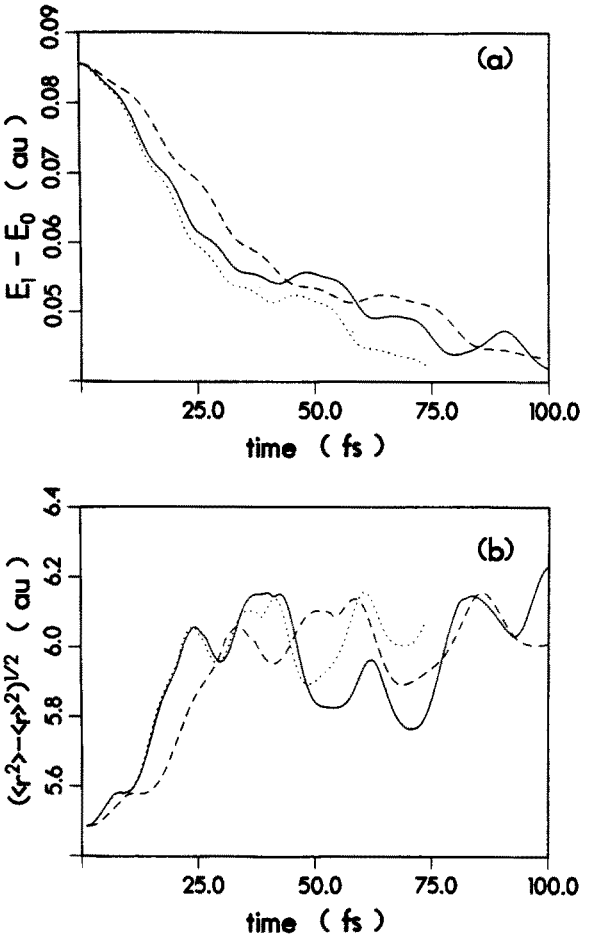

FIG. 7. (a) Time evolution of the energy gap $\Delta E = E_1 - E_0$ following sudden excitation at $t = 0$ from the ground to the first excited state of the solvated electron in $(H_2O)_{\bar{1}28}$ and $(D_2O)_{\bar{1}28}$ clusters. (b) Time evolution of the excited state width, $(\langle r^2\rangle - \langle r\rangle^2)^{1/2}$, during the same relaxation process. Solid lines: $(H_2O)_{\bar{1}28}$. Dashed lines: $(D_2O)_{\bar{1}28}$. Dotted lines: the $(D_2O)_{\bar{1}28}$ result with the time axis divided by $\sqrt{2}$. These results, as well as those exhibited in Figs. 8 and 9, were obtained by averaging the results of two simulations starting from different initial configurations. Note the similarity (in particular at short times following the excitation) between the results for $(H_2O)_{\bar{1}28}$ in this figure and those shown in Figs. 2 and 3 which were obtained by averaging over 5 trajectories. This comparison serves to indicate the adequate level of statistical significance of the results.

deuterium mass ratio. Very similar behavior was obtained in comparing the fast relaxation process following electronic excitation in $(H_2O)_{\bar{1}28}$ [Figs. 7(a) and 7(b)]. Due to the very limited amount of statistical averaging used in this calculation we could not determine whether the longer relaxation process shows a similar isotope effect. However, it is experimentally known[64] that the Debye (as well as the longitudinal) relaxation time in D_2O is longer by $\sim 20\%$ than the corresponding times in H_2O.

Further insight into the fast relaxation process is gained from Figs. 8 and 9 where we have divided the water molecules in the $(H_2O)_{\bar{1}28}$ cluster into three groups: group a (solid lines) includes those 6–7 molecules which at time $t = 0$, when the excitation to the upper electronic state occurs, were located within 7 a.u. from the center, $\langle r\rangle$, of the (ground-state) electronic wave function; group b (dashed lines) includes the 16–18 molecules which at $t = 0$ are located between 7 and 10 a.u. from the electron center and group c includes all the other molecules. The selection of the above shell radii was motivated by the solvation shell structure obtained in our previous studies,[60,56] of electron localization in water clusters. The time evolution of the interaction energy between the electron and the water molecules (per water molecule) and the water–water interaction potential energy (per molecule) for molecules in groups a and b are depicted in Figs. 8 and 9, respectively. Note that intermolecular interaction energy is calculated for the molecules in the group with all the other cluster molecules. No systematic time variation beyond the statistical noise has been seen for these quantities associated with the moecules in group c.

Figures 8 and 9 clearly show that the fast relaxation process following electronic excitation of a solvated electron is primarily dominated by molecules nearest to the center of the excess electron distribution. Figure 9 further indicates that the configurational changes that take place during this time are associated with rotations or librations of these water

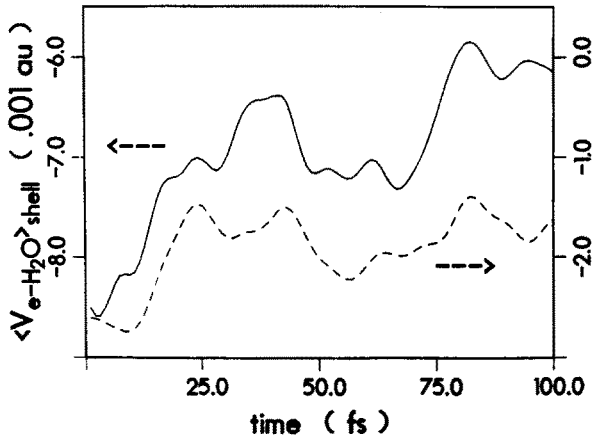

FIG. 8. Time evolution of the interaction energy (per water molecule) between the electron and the water molecules that were in the first solvation shell (0–7 a.u., solid line) and in the second solvation shell (7–10 a.u., dashed line), following a sudden transition from the ground to the first excited state of the solvated electron in $(H_2O)_{\bar{1}28}$.

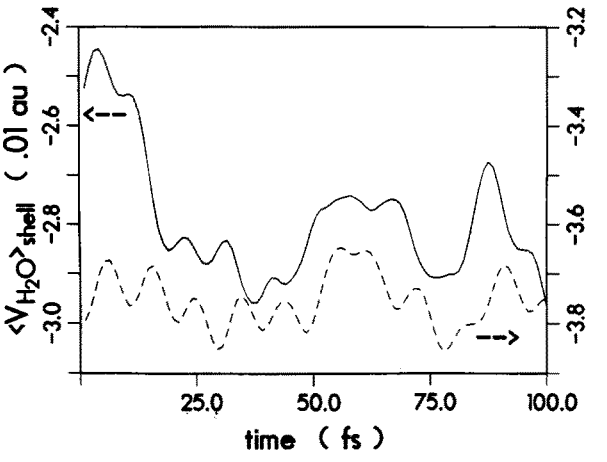

FIG. 9. Time evolution of the intermolecular potential energy (per molecule) between water molecules in the first solvation shell (0–7 a.u., full line) and the second solvation shell (7–10 a.u., dashed line) following excitation at $t = 0$ of $(H_2O)_{\bar{1}28}$.

molecules nearest to the electron. Thus, after the excitation, the electronic charge distribution is more diffuse, resulting in a weakening of the electron–water interaction, leading to a reorientational response of the molecules in the immediate vicinity of the excess electron which is accomplished via rotations of the molecules (involving motion of the hydrogen atoms in an attempt to increase the degree of hydrogen bonding and the magnitude of intermolecular interaction associated with them). That hydrogen bonding is disrupted in the first water molecules shell by the presence of the electron is seen (Fig. 9) by the fact that the intermolecular interaction (per molecule) associated with the molecules in the second (7–10 a.u.) shell is considerably larger than that associated with the first shell molecules. We note that Maroncelli and Fleming[16] have reached similar conclusions from the analysis of their classical simulation data.

The isotope effect seen in Figs. 6 and 7 is indicative of the nature of this rotational response mechanism. We recall[65] that the Debye dielectric relaxation time τ_D, obtained from a model of rotational diffusion is in our case independent of the rotator mass or its moment of inertia ($\tau_D = 4\pi\eta a^3/kT$ where η is the solvent viscosity and an appropriate choice for the "rotator radius" a is the OH bond length). On the other hand, the rotational correlation function of free rotators in thermal equilibrium decays in time as $\sim e^{-t^2(kT/I)}$ where I is the moment of inertia.[65] We suggest that the dependence on $\sqrt{m_D/m_H} = \sqrt{2}$ seen from the isotope effect corresponds to the inertial character of this short-time relaxation. It would be interesting to check whether the temperature dependence of the fast relaxation time scales like $T^{-1/2}$ as also suggested by the free rotator model. However, in the present study we did not accumulate enough statistics to make a reliable check of this point.

Several other points concerning the observed relaxation behavior should be noted.

(a) The dynamics of electron localization and Stokes shift (reorganization energy) evolution are not sensitive to the cluster size for the (relatively large) water clusters that support an internally solvated electron ($n \gtrsim 60$), at least to within the statistical accuracy of our result for the relaxation time scales which we estimate to be approximately $\pm$ 20%. In contrast, the ground and excited state energies shift to more negative values for larger clusters and therefore we expect the IR absorption discussed below [see (g) and (h)] to peak at higher frequencies for larger clusters.

(b) Figures 1 and 5(a) show that the excited state electronic energy is much less sensitive to the reorganization of the surrounding water configuration than the ground-state energy. This is in contrast to the pronounced change in the widths (Fig. 3) of both the ground and excited electronic states following the electronic excitation. Underlying the water relaxation after transition to the excited electronic state is the weaker interaction with the more diffuse excited electronic charge distribution. Thus, the water molecules change their orientation in order to lower the intermolecular interaction energy. This water relaxation affects the electronic energy in two opposing ways: First, the electron–water interaction energy (the electron potential energy) is weakened (i.e., becomes less negative), secondly the electron kinetic energy associated with the more diffuse wave function is smaller (less positive). The overall result is that there is only a very small net effect on the total excited state electronic energy.

(c) The similarity between the relaxation phenomena observed in the present work, in the electron localization simulation of Schnitker and Rossky,[53] and in the classical simulations of Refs. 15, 16, 51, and 63 is significant and surprising in view of the fact that not only different processes are studied but mainly because very different models of water were used. We use the RWK2-M water–water potential[58] and the pseudopotential developed by Barnett, Landman, and Jortner[60] for the water electron interaction. References 53 and 63 use the SPC water model while in Refs. 15 and 16 the ST2 water model was used. It appears that the inertial regime seen in all these simulations is not very sensitive to the details of the model used. This suggests that it is very probable that this behavior will be found in real water and perhaps in other associated solvents (with scaled character-

istic times). It should be kept in mind, however, that all these studies are characterized by a non-self-consistent treatment of the electronic polarization of the solvent water molecules and that including such many-body contributions[66] may have some effect on the short-time behavior.[44]

(d) Another important difference between the (quantum-mechanical) processes simulated in the present work (and in Ref. 53) and the classical simulations of Refs. 15 and 16 is the fact that in the latter group of studies the charge distribution is held fixed after its instantaneous formation at $t = 0$ while in the electronic localization and relaxation studies the electronic charge distribution varies during the relaxation, mostly during the initial fast period. The fact that the time scales obtained from the quantum-mechanical simulations are similar to those seen in the classical, fixed charge, studies again indicates that the dynamics is mainly driven by the inertial motion of the water molecules and that this motion is in a sense rate determining also in the electronic relaxation and localization process. It should be emphasized that the fact that the electron charge distribution relaxes to practically its final form during the initial fast part of the relaxation process justifies the use of fixed charge dielectric relaxation models for the longer time scales associated with electron localization, solvation, and transfer processes.

(e) Rao and Berne[15] and also Maroncelli and Fleming[16] have observed a very large jump of the average kinetic energy (temperature) of the classical atoms in the first solvation shell following the sudden charge formation. This local heating persists for a relatively long time (~ 0.5 ps). In our simulation where the sudden electronic excitation or relaxation involves a relatively mild change in the charge distribution no increase in the local temperature (beyond the noise level) was observed.

(f) Participation of intramolecular vibrational modes during the short-time stage of the relaxation processes discussed above cannot be ruled out. However, the similarity between the results obtained using our flexible water model and the other simulations which use rigid water molecules indicate that this relaxation channel does not play a major role in the process.

(g) It is interesting to speculate on the relation between the results obtained here and in Ref. 53 and the experimental results of Migus *et al.*[29] The fact that these authors do not observe a continuous blue shift of the absorption spectrum from the near IR to the 7000 Å range during the electron solvation process was interpreted by them (see also Ref. 53) as an indication of the existence of two species, one that absorbs in the near IR, and the other which is the fully solvated electron. It is reasonable to assign the IR absorbing species to the solvated electron in an excited state. Figure 10 gives a schematic view of the transitions involved. Our simulation results[67] give the peak of the excitation profile of the fully solvated electron at 2.2 eV and the vertical transition between the first excited state and the delocalized continuum at slightly above 1 eV. The experimental result[68] for the former is 1.72 eV and for the latter, 0.92 eV. The fact that our simulations tend to overestimate the transition energies lead us to suggest that the vertical transition from the excited states to the delocalized continuum may peak below 1 eV. In

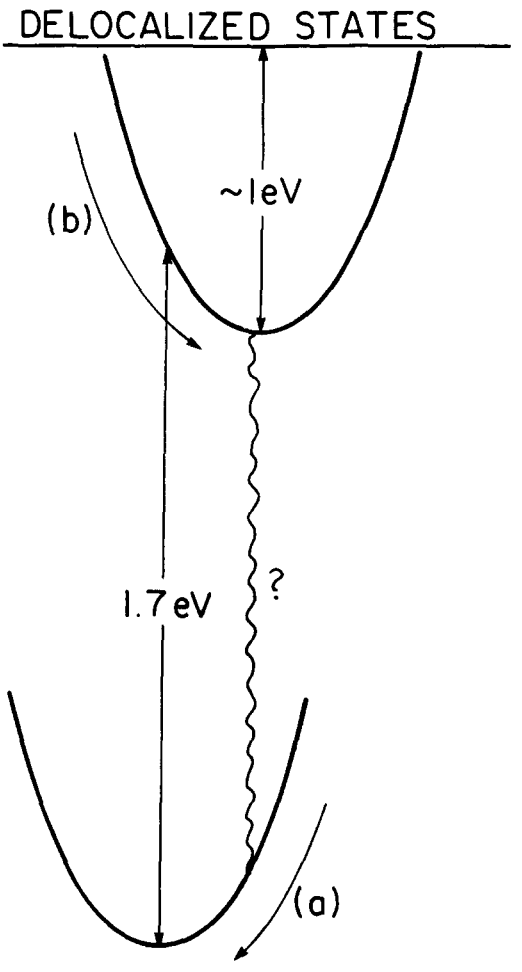

FIG. 10. A schematic description of a model for the time scales and energetics associated with the dynamics of electron solvation and excitation in water.

the present work we have determined the relaxation process (a) and (b) of Fig. 10 to occur on similar time scales and to involve at least two relaxation times ~ 30 and 200 fs. It is likely that the 110 fs process that Migus *et al.* attribute to the growth of the IR absorbing species actually reflects the evolution of a blue shift of the IR absorption by the excited state of the solvated electron, to the delocalized continuum, *during* relaxation process (b). The time (240 fs) observed by these workers for the decay of the IR absorbing species and the buildup of the fully solvated electron is probably due to the relaxation process (a) in Fig. 10, or to a radiationless transition from the excited to the ground state (denoted by a question mark in Fig. 10) or to a combination of both. It will be highly desirable to determine from the theoretical model the rate of this nonadiabatic radiationless process.

(h) The model described above and the simulation results of this paper lead us to predict that following excitation of the solvated electron in water one should be able to observe a transient IR absorption that will peak below 1 eV and will decay on the 240 fs time scale observed by Migus *et al.* This absorption should in principle blue shift on a time scale characterized by a 20–30 fs process and a slower ~ 200 fs process [process (b) of Fig. 10]. The short-time blue shift will be sensitive to deuterium isotope substitution of the wa-

ter in the way described above. We should note, however, that the very weak dependence of the excited state energy E_1 on the solvent reorganization following the ground to excited state transition [see point (b) above] suggests that this blue shift may be too weak to observe.

(i) A substantial part of the water relaxation in response to the charge reorganization (electron excitation or localization as well as classical charge formation) observed here and in other works, is beyond the prediction of current theoretical treatments of solvation dynamics. It is highly significant that the classical simulation by Maroncelli and Fleming[50] indicate that the essential features of this phenomenon can be described within linear response theory. This suggests that a linear response based calculation of the wave vector and frequency-dependent dielectric response $\epsilon(k,\omega)$ for associated liquids should be a sufficient theoretical framework for describing this phenomenon. A recent calculation[45] of $\epsilon(k,\omega)$ for a model of polarizable atoms on a lattice (as an approximation for a nonassociated solvent) yields only the (nonexponential) slow time scale relaxation with characteristic times between τ_D and $\epsilon_L = (\epsilon_\infty/\epsilon_0)\tau_D$. This indicates the importance of structural reorganization within the first solvation shell characteristic of associated solvents in the initial fast stage of the relaxation.

CONCLUSIONS

We have simulated the dynamics of the solvated electron in water and in D_2O following sudden transitions between its ground and the first excited states. A very fast ($\sim$20–30 fs) and a slower ($\sim$200 fs) relaxation processes were observed. The short-time evolution is attributed to hydrogen atom rotation in the inertial regime, mostly associated with water molecules in the first solvation shell about the electron. The longer time scales are of the same order as the longitudinal dielectric relaxation time in water. A model based on our results and on the experimental results of Migus *et al.* predicts that a transient IR absorption should be observed following optical excitation of the solvated electron, that may blue shift and decay on the time scales 20–200 fs. The short (20–30 fs) time scale is predicted to depend on deuterium isotope substitution of the water [$(\tau(D_2O)/\tau(H_2O)\sim\sqrt{2}$].

ACKNOWLEDGMENTS

This work is supported by the U.S. Department of Energy under Grant No. DE-FG05-86ER-45234, the US–Israel Binational Science Foundation (to U.L. and A.N.), and the Commission for Basic Research of the Israel Academy of Science (to A.N.). Comments on the manuscript by J. Jortner and I. Rips are gratefully acknowledged.

APPENDIX

1. The adiabatic simulation method (ASM)

As mentioned in the introduction, while it is possible to implement the time-dependent self-consistent-field (TDSCF) formulation for studies of real-time dynamics of a quantum subsystem coupled to dynamical classical degrees of freedom,[55,56] in our present investigations we limit ourselves to the adiabatic time evolution of such a coupled quantum–classical system (i.e., excess electron interacting with a classical polar cluster). This adiabatic simulation method[55,56] (ASM, and its ground-state dynamics, GSD, version) affords a significant reduction in computational time for processes which are essentially adiabatic as compared to the full real-time dynamical evolution. Clearly the method is suited for situations where the subsystems, comprising the system, are characterized by widely separated time scales, such as the situations normally treated by the adiabatic or Born–Oppenheimer approximation. In fact, by construction the method is a numerical implementation of the adiabatic approximation where the electron (fast subsystem) is assumed (and is constrained) to remain at all times in a specified eigenstate of the Hamiltonian corresponding to the instantaneous configuration of the classical particles (the slow subsystem). Thus, denoting by $\{\mathbf{R}_i(t)\}$ the collection of coordinates of the classical particles, the Hamiltonian for the excess electron can be written as

$$\hat{H}(t) = \hat{K} + \hat{V}(\{\mathbf{R}_i(t)\}), \tag{A1}$$

where $\hat{K}$ and $\hat{V}$ are the kinetic and potential energy operators. The eigenstates of this Hamiltonian are the solutions to the Schrodinger equation

$$\hat{H}(t)|\psi_l(\{\mathbf{R}_i(t)\})\rangle = E_l(t)|\psi_l(\{\mathbf{R}_i(t)\})\rangle, \quad l=0,1,2,\ldots . \tag{A2}$$

In the mixed quantum classical version of the TDSCF approximation the dynamical evolution of the classical particles obeys Newton's equations

$$M_j\ddot{\mathbf{R}}_j = \mathbf{F}_j - \nabla_{\mathbf{R}_j}U(\{\mathbf{R}_i\}), \quad j=1,\ldots,N_c, \tag{A3}$$

where N_c is the number of classical particles, $U(\{\mathbf{R}_i\})$ is the interparticle interaction potential, and the force $\mathbf{F}_j$ is evaluated via the Hellmann–Feynman theorem:

$$\mathbf{F}_j = -\int d\mathbf{r}\,\psi_l^* \times\left[\mathbf{r};\{\mathbf{R}_i(t)\}\left[\nabla_{\mathbf{R}_j}V(\mathbf{r},\{\mathbf{R}_i(t)\})\right]\psi_l(\mathbf{r},\{\mathbf{R}_i(t)\})\right], \tag{A4}$$

where the integration is over the electronic coordinates and V is the interaction potential between the electron and the atomic constituents.

The desired state $|\psi_l(t)\rangle$ (where the explicit dependence on $\{\mathbf{R}_j\}$ has been dropped) can be obtained from an arbitrary state $|\psi\rangle$ (assuming that the two are not orthogonal [i.e., $\langle\psi_l(t)|\psi\rangle\neq 0$] by the operation

$$\lim_{\beta\to\infty} e^{-\beta\hat{H}(t)}\hat{P}_l(t)|\psi\rangle \to \langle\psi_l(t)|\psi\rangle e^{-\beta E_l(t)}|\psi_l(t)\rangle, \tag{A5}$$

where the projection operator, $\hat{P}_l(t)$, is given by

$$\hat{P}_l(t) = 1 - \sum_{m=0}^{l-1}|\psi_m(t)\rangle\langle\psi_m(t)| \quad (l\neq 0), \tag{A6}$$

and $\hat{P}_0(t)\equiv 1$ for the ground state ($l=0$, which is the case in GSD). As seen from Eq. (A5), determination of an excited state l, requires the prior determination of all the lower energy eigenstates. Note also that the operation in Eq. (A5) can be regarded as evolution of the wave function in imaginary time $t = -i\beta$. This fact is conveniently used in converting the computer programs[55,56] from performing real-time evo-

lution of the wave function to the operation described by Eq. (A5).

The above equations define the adiabatic simulation method (ASM). For an alternative description see Refs. 55 and 56. The numerical implementation of the operation on the left-hand side (LHS) of Eq. (A5) is achieved by the split-operator fast Fourier transform (FFT) method.[61] First, denoting $|\tilde{\psi}\rangle_l = \hat{P}_l(t)|\psi\rangle$, the LHS of Eq. (A5) can be written as

$$e^{-\beta\hat{H}}|\tilde{\psi}\rangle_l = \lim_{J\to\infty}\prod_{j=1}^{J}(e^{-\beta\hat{K}/2J}e^{-\beta\hat{V}/J}e^{-\beta\hat{K}/2J})|\tilde{\psi}\rangle_l \tag{A7}$$

Evaluation of the RHS of Eq. (A7) proceeds by performing the $\hat{K}$ and $\hat{V}$ operations in the momentum and coordinate spaces, respectively (since the kinetic energy operator is diagonal in the momentum representation and the potential energy operator is diagonal in the coordinate representation). At this stage the wave function and potential are defined on a grid with periodic boundary conditions, and the FFT method is used to switch between the coordinate and momentum representations of the wave function. In these calculations an error proportional to $\Delta\beta^3$, where $\Delta\beta = \beta/J$, is introduced due to the noncommutativity of the kinetic and potential energy operators. Also, in pracitcal applications, the projection operation, Eq. (A6), is performed several times during the imaginary time evolution, Eq. (A7), in order to avoid the growth of lower state amplitudes due to numerical errors. In addition we note that the grid representation, introduced in connection with the FFT, restricts the spatial resolution (determined by the mesh size) and the momentum (and thus the kinetic energy) range which can be described.[61]

2. Application to finite systems

The introduction of the grid representation for the wave function and interaction potential between the quantum particle and the atoms $[V(\mathbf{r},\{\mathbf{R}_i\})]$ implies a spatial periodicity of these quantities determined by the dimensions of the grid. In order to use the method for studies of a finite system (or in general for systems characterized by nonperiodic potentials) and in particular in studies of localized states, one must assure that the amplitude of the wave function under study as well as the amplitudes of the wave functions corresponding to lower energy eigenvalues, vanish at the surface of the grid. These conditions can be satisfied for any localized state by simply assuring that the spatial extent of the employed grid is large enough. This can be accomplished by either increasing the number of grid points or by increasing the grid spacing. However, an increase in the number of grid points results in increased computation time, while increasing the grid spacing decreases the spatial resolution and (consequently) the energy range that can be accounted for.

In the problem we wish to study in this paper and in studies of electron migration,[57] the excess electron density, $\rho(\mathbf{r})$, is localized but its spatial extent and position may change in time. To facilitate the application of the FFT–GSD method to this problem we have developed an efficient "moving grid" algorithm in which the position and spatial extent of the density are monitored and the grid is adjusted accordingly. The algorithm is outlined below.

(1) At time t we have the positions and velocities of the atomic constituents of the molecular cluster, $\{\mathbf{R}_i(t)\}$ and $\dot{\mathbf{R}}_i(t)\}$, and the wave function of the specified state l, $\psi(\mathbf{r},t)\equiv\psi_l(\mathbf{r};\{\mathbf{R}_i(t)\})$ which is defined only at the grid points. The grid point positions are denoted by $\mathbf{r}_{lmn} = \mathbf{r}_0 + (l,m,n)\Delta$ where Δ is the grid spacing and $\mathbf{r}_0$ is the vector defining the origin of the grid. The amplitude of the wave functions at the grid points is $\psi_{lmn}(t)$, and the wave function is normalized, i.e., $\Sigma_{l,m,n}\psi^*_{lmn}(t)\psi_{lmn}(t) = \Delta^{-3}$.

(2) Compute the center of density

$$\mathbf{r}_e = \Delta^3\sum_{l,m,n}\mathbf{r}_{lmn}\psi^*_{lmn}\psi_{lmn}, \tag{A8}$$

and the density weighted grid surface-to-volume ratio,

$$\gamma = 1 - \Delta^3\sum_{l,m,n=-N/2+2}^{N/2-1}\psi^*_{lmn}\psi_{lmn}. \tag{A9}$$

(a) If γ is larger than a cutoff value $\gamma_{\max}$ (chosen as 2.5% of the uniformly weighted grid surface to volume ratio which for a cubic grid, containing N^3 points, is given by $[N^3-(N-2)^3]/N^3$) then the simulation is stopped and is restarted with either a larger N or Δ. Conversely when $\gamma \ll \gamma_{\max}$ it is beneficial to decrease Δ and/or N.

(b) If any component of $\mathbf{r}_e - \mathbf{r}_0$ is larger in magnitude than Δ, the grid is moved by one grid spacing in the appropriate direction and the new grid points (i.e., on the surface of the grid) are assigned zero wave function amplitudes.

(3) Compute the electron-cluster interaction potential at the grid point, $V(\mathbf{r}_{lmn})$ and the derivatives with respect to nuclear coordinates, $\partial V(\mathbf{r}_{lmn})/\partial\mathbf{R}_i$. The potential felt by the electron at time $t+\Delta t$ is estimated by

$$V(t+\Delta t,\mathbf{r}_{lmn}) \simeq V(t,\mathbf{r}_{lmn}) + \sum_{i=1}^{N_c}\times[\partial V(t,\mathbf{r}_{lmn})/\partial\mathbf{R}_i]\cdot\dot{\mathbf{R}}_i\Delta t. \tag{A10}$$

The forces on nuclei resulting from the electron-molecule interaction are obtained from Eq. (A4).

(4) The wave function at the grid points is updated to $\psi_{lmn}(t+\Delta t)$ using Eqs. (A5) and (A7) [with $\psi_{lmn}(t)$ in place of the arbitrary function ψ) and using the estimated potential $V(t+\Delta t,\mathbf{r}_{lmn})$.

(5) The intramolecular and intermolecular potentials and forces are computed, and the nuclear positions and forces are evolved to time $t+\Delta t$, using Eq. (A3).

Note that the use of the estimated interaction potential $V(t+\Delta t)$, Eq. (A10), allows us to eliminate a separate loop over grid points and molecules. Another alternative would be to compute the forces on the nuclei at time t from $\psi(t-\Delta t)$, but this requires a much smaller time increment, Δt, in order to conserve the total energy over a lengthy simulation. The "moving grid" part of the algorithm [step (2)] allows us to use a smaller grid spacing (Δ) and/or number of grid points (N^3).

[1] J. B. Hubbard and P. G. Wolynes, in *Physics of Ionic Solvation*, edited by Ulstrup (Elsevier, Amsterdam, 1986).

[2] See, for example, the papers in Faraday Discuss. Chem. Soc. **85** (1988) for a survey of current areas of research.

[3]E. M. Kosower and B. Huppert, Ann. Rev. Phys. Chem. **37**, 127 (1986).
[4]W. R. Ware, S. K. Lee, and P. Chow, Chem. Phys. Lett. **2**, 356 (1968).
[5]W. R. Ware, S. K. Lee, C. J. Brandt, and P. P. Chow, J. Chem. Phys. **54**, 4729 (1971).
[6]L. A. Hallidy and M. R. Topp. Chem. Phys. Lett. **48**, 41 (1977).
[7]Yu. T. Mazurenko and V. S. Udaltsov, Opt. Spectrosc. (USSR) **44**, 417 (1978).
[8]T. Okamura, M. Sumitani, and K. Yoshihara, Chem. Phys. Lett. **94**, 339 (1983).
[9]S. W. Yeh, L. A. Phillips, S. P. Webb, L. F. Buhse, and J. H. Clark, in *Ultrafast Phenomena IV*, edited by D. H. Auston and K. B. Eisenthal (Springer, Berlin, 1984), p. 359.
[10]M. Maroncelli and G. R. Fleming, J. Chem. Phys. **86**, 6221 (1987).
[11]V. Nagarajan, A. M. Brearley, T. J. Kang, and P. F. Barbara, J. Chem. Phys. **86**, 3183 (1987).
[12]M. A. Kahlow, T. J. Kang, and P. R. Barbara, J. Phys. Chem. **91**, 6452 (1987).
[13]M. A. Kahlow, T. J. Kang, and P. F. Barbara, J. Chem. Phys. **88**, 2372 (1988).
[14]D. F. Calef and P. G. Wolynes, J. Phys. Chem. **87**, 3387 (1983), and J. Chem. Phys. **78**, 470 (1983).
[15]M. Rao and B. J. Berne, J. Phys. Chem. **85**, 1498 (1981).
[16]M. Maroncelli and G. R. Fleming, J. Chem. Phys. **89**, 5044 (1988).
[17]W. S. Struve and P. M. Rentzepis, Chem. Phys. Lett. **29**, 23 (1974); J. Chem. Phys. **60**, 1533 (1974).
[18]D. Huppert, S. D. Rand, P. M. Rentzepis, P. F. Barbara, W. S. Struve, and Z. R. Grabowski, J. Chem. Phys. **75**, 5714 (1981).
[19]Y. Wang, M. McAuliffe, F. Novak, and K. B. Eisenthal, J. Phys. Chem. **85**, 3736 (1981).
[20]D. Huppert, H. Kanety, and E. M. Kosower, Discuss. Faraday Soc. (London) **74**, 161 (1982).
[21]E. M. Kosower and D. Huppert, Chem. Phys. Lett. **96**, 433 (1983).
[22]D. Huppert, V. Ittah, and E. M. Kosower, Chem. Phys. Lett. **144**, 15 (1988).
[23]E. W. Castner, Jr., M. Maroncelli, and G. R. Fleming, J. Chem. Phys. **86**, 1090 (1987).
[24]S. G. Su and J. D. Simon, J. Phys. Chem. **90**, 6475 (1986); **91**, 2693 (1987); J. D. Simon and S. G. Su, J. Chem. Phys. **87**, 7016 (1987).
[25]H. Heitele, M. E. Michel-Beyerle, and P. Finckh, Chem. Phys. Lett. **138**, 237 (1987).
[26]J. H. Baxendale and P. Wardman, Nature **230**, 449 (1971); J. Chem. Soc. Faraday Trans. 1 **69**, 584 (1973); Can. J. Chem. **55**, 1996 (1977).
[27]W. J. Chase and J. W. Hunt, J. Phys. Chem. **79**, 2835 (1975).
[28]G. A. Kenney-Wallace and D. C. Jonah, Chem. Phys. Lett. **39**, 596 (1976); J. Phys. Chem. **86**, 2572 (1982).
[29]A. Migus, Y. Gauduel, J. L. Martin, and A. Antonetti, Phys. Rev. Lett. **58**, 1559 (1987).
[30]H. Miyasaka, H. Masuhara, and N. Mataga, Laser Chem. **7**, 119 (1987).
[31]G. A. Kenney-Wallace, G. E. Hall, L. A. Hunt, and K. Sarantidis, J. Phys. Chem. **84**, 1145 (1980).
[32]H. Sumi and R. A. Marcus, J. Chem. Phys. **84**, 4894 (1986)– W. Nadler and R. A. Marcus, *ibid.* **86**, 3906 (1987).
[33]J. P. Bergsma, B. J. Gertner, K. R. Wilson, and J. T. Hynes, J. Chem. Phys. **86**, 1356 (1987).
[34]B. J. Gertner, J. P. Bergsma, K. R. Wilson, S. Lee, and J. T. Hynes, J. Chem. Phys. **86**, 1377 (1987).
[35]I. Rips and J. Jortner, J. Chem. Phys. **87**, 2090 (1987).
[36]D. A. Zichi and J. T. Hynes, J. Chem. Phys. **88**, 2513 (1988).
[37]M. Sparpaglione and S. Mukamel, J. Chem. Phys. **88**, 3263 (1988).
[38]Yu. T. Mazurenko. Opt. Spectrosc. (USSR) **36**, 283 (1974).
[39]B. Bagchi, D. W. Oxtoby, and G. R. Fleming, Chem. Phys. **86**, 257 (1984).
[40]G. van der Zwan and J. T. Hynes, J. Phys. Chem. **89**, 4181 (1985).
[41]R. F. Loring, Y. J. Yan, and S. Mukamel, Chem. Phys. Lett. **135**, 23, (1987).
[42]E. W. Castner, Jr., B. Bagchi, and G. R. Fleming, Chem. Phys. Lett. **143**, 270 (1988).
[43]E. W. Castner, Jr., G. R. Fleming, B. Bagchi, and M. Maroncelli, J. Chem. Phys. **89**, 3519 (1988).
[44]D. F. Calef and P. G. Wolynes, J. Chem. Phys. **78**, 4145 (1983).
[45]R. F. Loring and S. Mukamel, J. Chem. Phys. **87**, 1272 (1987); R. F. Loring, Y. T. Yan, and S. Mukamel, *ibid.* **87**, 5840 (1987).
[46]V. Friedrich and D. Kivelson, J. Chem. Phys. **86**, 6425 (1987).
[47]P. G. Wolynes, J. Chem. Phys. **86**, 5133 (1987).
[48]I. Rips, J. Klafter, and J. Jortner, J. Chem. Phys. **88**, 3246 (1988); **89**, 4288 (1988).
[49]A. L. Nicholls III and D. F. Calef, J. Chem. Phys. **89**, 3783 (1988).
[50]M. Maroncelli and G. R. Fleming, J. Chem. Phys. **89**, 875 (1988).
[51]S. Engstrom, B. Jonsson, and R. W. Impey, J. Chem. Phys. **80**, 5481 (1984); S. Engstrom, B. Jonsson, and B. Jonsson, J. Magn. Reson. **50**, 1 (1982).
[52]O. A. Karim, A. D. J. Haymet, M. J. Banet, and J. D. Simon, J. Phys. Chem. (submitted).
[53]P. J. Rossky and J. Schnitker, J. Phys. Chem. **92**, 4277 (1988).
[54]J. Schnitker, K. Motakabbir, P. J. Rossky, and R. Friesner, Phys. Rev. Lett. **60**, 456 (1988).
[55]R. N. Barnett, U. Landman, and A. Nitzan, Phys. Rev. A **38**, 2178 (1988).
[56]R. N. Barnett, U. Landman, and A. Nitzan, J. Chem. Phys. **89**, 2242 (1988).
[57]R. N. Barnett, U. Landman, and A. Nitzan, Phys. Rev. Lett. **62**, 106 (1989).
[58]J. R. Reimer and R. O. Watts. Chem. Phys. **85**, 83 (1984); **64**, 95 (1982).
[59]R. N. Barnett, U. Landman, C. L. Cleveland, and J. Jortner, Phys. Rev. Lett. **59**, 811 (1987); J. Chem Phys. **88**, 4421 (1988).
[60]R. N. Barnett, U. Landman, C. L. Cleveland, and J. Jortner, J. Chem. Phys. **88**, 4429 (1988); Chem. Phys. Lett. **145**, 382 (1988).
[61]M. D. Feit, J. A. Fleck, Jr., and A. Steiger, J. Comput. Phys. **47**, 412 (1982); M. D. Feit and J. A. Fleck, Jr., J. Chem. Phys. **78**, 301 (1983); **80**, 2578 (1984); see the review by R. Kosloff, J. Phys. Chem. **92**, 2087 (1988).
[62]M. Sprik and M. L. Klein, J. Chem. Phys. **89**, 1592 (1988).
[63]D. Chandler, reported in the ACS Meeting, Los Angeles, 1988.
[64]C. H. Collie, J. B. Hasted, and D. M. Ristoy, Proc. Phys. Soc. London **60**, 145 (1948).
[65]C. J. G. Bottcher and P. Bordewijk, *The Theory of Electric Polarization* (Elsevier, Amsterdam, 1978), Vol. II, Chap. 11.
[66]A. Wallqvist, D. Thirumalai, and B. J. Berne, J. Chem. Phys. **86**, 6404 (1987).
[67]R. N. Barnett, U. Landman, and A. Nitzan, Ref. 56; and J. Chem. Phys. (submitted).
[68]E. J. Hart and W. C. Gottschall, J. Am. Chem. Soc. **71**, 2101 (1969).